Investigation of typical and atypical functional activation patterns in Autism Spectrum Disorder

Ferran Gonzalez Hernandez[1]*, Paola Pinti [2], Ilias Tachtsidis[2]

Abstract
Multivariate pattern analyses (MVPA) have been extensively used in functional magnetic resonance imaging (fMRI) to simultaneously analyse the information contained in different areas of the brain. However, just a few studies have started to apply these techniques to functional near infrared spectroscopy (fNIRS). fNIRS is a neuroimaging technique that measures the same physiological signal as fMRI but with fewer constraints on the environmental set-ups in which experiments can be performed. Here, MVPA were applied to fNIRS data from 27 typically developed (TD) participants and 26 high-functioning participants with autism spectrum disorder (ASD) during prospective memory tasks. Representational similarity analyses were used to compare the signal of each individual to the average of subjects with the same condition (either TD or ASD). The results obtained exhibited the capacity of the algorithm to quickly assess those features of the hemodynamic response that were more informative and compare the results from both oxy- and deoxy hemoglobin.

[1] *CoMPLEX, University College London, London, United Kingdom*
[2] *Biomedical Optics Research Laboratory, Department of Medical Physics & Biomedical Engineering, University College London, London, United Kingdom*
*__Email__: ferran.hernandez.17@ucl.ac.uk

Contents

1. Introduction

Autism Spectrum Disorder (ASD) is a neurodevelopmental condition characterized by deficits in social interaction and communication as well as restricted, repeated, and stereotyped interest and behaviour [1, 2]. Despite extensive research, the complex aetiology and neurobiology of ASD limits its effective treatment and diagnosis [3]. The increasing prevalence of this condition worldwide requests improvements towards a better understanding and diagnosis of the disease. Nowadays, ASD is merely diagnosed through clinical interviews and behavioural observations, which often leads to misdiagnosed subjects and unsuccessful treatments. Since the same behavioural phenotypes can be the result of different biological conditions, successful characterization of ASD is likely to require an integrative platform, where behavioural information is combined with neuroimaging data [4].

Previous studies using functional magnetic resonance imaging (fMRI) and diffusion tensor imaging (DTI) have already reported neurobiological differences between typically developed (TD) and ASD subjects [5]. Most of these studies described differences in neural activation in the prefrontal cortex (PFC) when subjects performed executive functions tasks (EF tasks, which include inhibition, working memory, sentence memory, planning, fluency, and shifting) [6]. However, evidence from different studies has often been conflicting. The inconsistency of results has been argued to be caused by heterogeneity in patient groups and the variety of EF tasks performed in each study [6]. However, another major factor has been the environmental conditions under which these studies were performed. Conventional neuroimaging techniques like fMRI or electroencephalography (EEG) are highly sensitive to body movements and impose restrictions on the experimental set-ups under which the studies can take place (e.g. fMRI scanner). Moreover, behavioural differences in EF tasks have mostly become evident in those scenarios that better mimic daily life situations, which are extremely hard to recreate in

the fMRI scanner.

Therefore, functional near-infrared spectroscopy (fNIRS) represents a particularly suited neuroimaging technique for the study of ASD. fNIRS is a relatively new and increasingly used method in neuroimaging studies that measures concentration changes of oxygenated (HbO_2) and deoxygenated (HHb) hemoglobin associated to neural activity. One of the main advantages of fNIRS in front of fMRI or EEG is its robustness against motion artifacts. Moreover, fNIRS devices are cheaper, portable and do not impose as many physical constraints, which enables the study of EF tasks in environments that better mimic real-life situations [7]. This is therefore one of the first studies in which neural activity of ASD patients is recorded through fNIRS when performing EF tasks. Subsequently, details about fNIRS signal and recording will be explained.

1.1 Functional Near-Infrared Spectroscopy

Like fMRI, fNIRS relies on the principle of neuro-vascular coupling (or hemodynamic response), which states that local neural activity is related to subsequent changes in cerebral blood flow [8]. The relative transparency of biological tissue on the near-infrared range (700-1000nm) allows fNIRS to measure the hemodynamic response by placing light sources and photodetectors over the tissue and analyse the amount of light absorbed. In the near-infrared range, most variation in physiological absorption is caused by HbO_2, HHb and cytochrome oxydase (Figure 1). Since hemoglobin is an oxygen carrier, increases in HbO_2 and decreases in HHb can be related to neural oxygen demand when a certain area of the brain is activated [7].

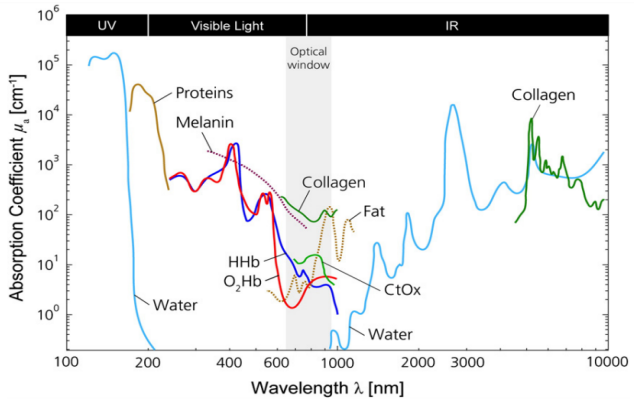

Figure 1. Absorption spectra relative to specific concentration (mM) for different compounds present in human tissue. Figure extracted from [9].

fNIRS measurments are performed by first placing light emitters and photodetectors at a certain distance to each other (3-4 cm). Then, photons are emitted by the source and travel through the biological tissue, where they can either be absorbed or back-scattered towards the detector. The banana-shape path shown in Figure 2 represents the probability that a photon travels from the emitter to the photodetector. By increasing the distance source-detector the penetration depth can be increased, but this can also affect the quality of the signal [7]. Pairs of optical fibers linking an emitter and a detector are referred as channels and they are placed at the mid-point between source-detector.

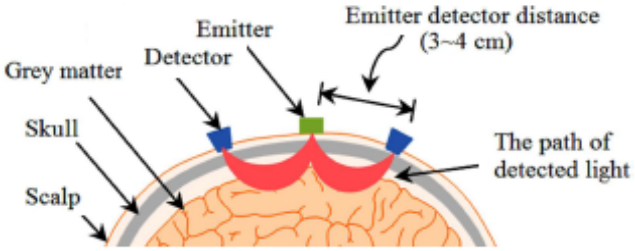

Figure 2. Emiter-detector pairs showing the banana-shaped path of near-infrared light during fNIRS recording. Figure adapted from [10].

During fNIRS recordings light is emitted at two different wavelengths (≈ 700 and ≈ 830nm) in order to detect changes in both HbO_2 and HHb. In the case of scattering mediums the modified Beer Lambert Law (MBLL) is used to translate changes in light intensity to optical density or attenuation (OD). According to the MBLL and assuming constant scattering, a change in optical density (ΔOD) can be described as:

$$\Delta OD(\Delta t,\lambda) = -log\frac{I(t_1,\lambda)}{I_0(t_0,\lambda)} = \sum_i \varepsilon_i(\lambda)\Delta c_i DPF(\lambda)d \quad (1)$$

In Equation 1 [9], DPF(λ) is the differential pathlength factor, I_0 and I are the emitted and transmitted lights at a source-detector separation d. $\varepsilon_i(\lambda)$ refers to the extinction coefficient of a certain compound (concentration c_i) at a specific wavelength (λ), and the i index denotes the investigated chromophores. Then, concentration changes of HbO_2 and HHb can be obtained by measuring changes in optical density at two wavelengths (λ_1, λ_2) and solving the following equation [9]:

$$\begin{bmatrix}\Delta[HHb]\\ \Delta[HbO_2]\end{bmatrix} = d^{-1}\begin{bmatrix}\varepsilon_{HHb\lambda_1}\varepsilon_{HbO_2\lambda_1}\\ \varepsilon_{HHb\lambda_2}\varepsilon_{HbO_2\lambda_2}\end{bmatrix}^{-1}\begin{bmatrix}\Delta OD(\lambda_1)/DPF(\lambda_1)\\ \Delta OD(\lambda_2)/DPF(\lambda_2)\end{bmatrix} \quad (2)$$

1.2 Previous studies and Multivariate Pattern Analysis (MVPA)

Given that fNIRS is far less intrusive than most traditional techniques, several studies have started employing it to investigate characteristics of early development and elderly populations. For example, a few studies have applied fNIRS to

study children with ASD. Yasumura et al. 2012 [11] and Xiao et al. 2012, [12] used fNIRS devices to monitor the neural signal over the PFC in TD and ASD children when performing several EF tasks. Yasumura et al. 2012 reported that TD children exhibited bilateral activation of the PFC whereas ASD children did not show right prefrontal activation during the experiment. Moreover, Xiao et al. 2012 reported a similar result, where ASD children displayed weaker right prefrontal activation than ASD during some of the tasks performed. Although this evidence is not enough to extract general conclusions, these studies already showed the capacity of using fNIRS in the study of ASD children.

For these analyses, fNIRS signals were compared between groups by performing student's t-test for each channel at a time, aiming to detect significant activations and comparing the results between groups. However, this type of analyses provide little information when trying to develop biomarkers for certain pathologies at the individual level. Given the high degree of neural variability across clinical populations, identifying conditions at the individual level represents a much more challenging task [6]. For this reason, new techniques have been developed over the last years to account for the information of multiple channels (or voxels in fMRI) at the same time, which are called multivariate pattern analyses (MVPA). In the field of fMRI, the emergence of such techniques allowed researchers to analyse activation patterns of multiple voxels (volumetric pixels from fMRI images) at a time instead of focusing on individual voxels. Particularly, in cognitive neuroscience, MVPA have been extensively used in fMRI studies to relate specific cognitive states with certain patterns of neural activity [13]. In fact, several studies have shown the higher sensitivity of MVPA, which was able to 'decode' (identify) certain neural states while traditional univariate methods with the general linear model (GLM) failed to do so. As an example, Gilber et al. 2009 [6] showed how, in some cases, conventional fMRI analyses were unable to distinguish between TD and ASD during certain tasks, whereas significant group differences were detected when applying MVPA.

Despite its acceptance in fMRI, the application of MVPA to fNIRS data has been much more limited. One of the main reasons for this fact is the lower spatial resolution of fNIRS in front of fMRI. While fMRI images are composed by thousands of voxels, the number of fNIRS recording sites is limited to 10-50 channels [14]. However, another major factor limiting the application of MVPA to fNIRS is the relative novelty of this technique as a neuroimaging modality, which still requires the development of analytical techniques comparable to the ones established in the fMRI community.

On the other hand, a few studies have already applied MVPA and machine learning approaches to fNIRS signals [15, 16, 17]. Ichikawa et al. 2014 [18] tried to classify between ADHD and ASD patients with fNIRS recordings during face processing tasks. In this study, Support Vector Machine (SVM) was applied to classify subjects depending on their hemodynamic response. SVMs are machine learning algorithms that try to maximize the margin between classes by seeking a set of weights for the input features. Despite reporting a classification accuracy of 84 % , this was only achieved when using the signal of a specific subset of channels as an input for the SVM, out of the 16,777,325 subsets analysed. However, when including all channels, classification accuracy was 62%. Therefore, a general methodology for classification might include a previous selection of relevant channels rather than the computationally exhaustive task of training as many SVMs (which are normally time-consuming on the training stage) as possible permutations of channels.

It is worth noting that all the fNIRS studies previously mentioned just reported HbO_2 as an index of brain activation. Although high correlation has been observed between the BOLD (Blood-Oxygen-Level-Dependent) signal of fMRI and the oxygenated hemoglobin recorded in fNIRS [2], analysing and reporting results from deoxygenated hemoglobin can also provide significant information. First, some studies have shown that for high signal-to-noise ratio in the measurements, HHb better correlated with BOLD signals [19]. Moreover, HbO_2 has been shown to be more influenced by motion artifacts than HHb, which makes this signal particularly valuable to assess the quality of the recordings. Finally, analysing and reporting results from both signals will help the fNIRS community to interpret not only the hemodynamic response in a more robust manner, but also the physiological events behind certain signals [8].

1.3 Context and experimental aims

This report expands on work previously carried out by the research group. A field experiment was performed in 27 TD and 26 ASD subjects, which were asked to perform certain EF tasks while their neural signal was recorded using fNIRS devices. During the experiments, participants performed prospective memory (PM) tasks, a type of EF that involves remembering to execute a previously formed intention at some future point [7]. Data was then pre-processed to remove motion artifacts and physiological noise. Moreover, initial analyses looked at behavioural differences between groups, and conventional channel-wise t-test were performed to detect significant differences between groups using block-averaged data. However, none of these reported significant differences.

Therefore, for this study MVPA were applied to the fNIRS data, aiming to detect characteristic differences that were not found with conventional univariate methods. With this approach, it was studied whether participants could be classified (as either TD or ASD) at the individual-level depending on their hemodynamic response when performing a PM task. Recently, Emberson et al. 2017 [14] reported neural decoding

in infants by applying a Representational Similarity Analysis (RSA) technique to fNIRS signal. RSA approaches use representational similarity structures to classify new observations by comparing their similarity to other known observations. As the RSA approach used in Emberson et al. 2017 enabled an easy interpretation, was computationally fast and was proposed as a platform for other fNIRS studies, it was implemented for decoding ASD vs TD subjects. This approach aimed to look at spatial distributions and relevant channels, as the signal from all possible combinations of channels could be analysed in a fast way. For this study, the application of the RSA was extended also to the HHb signal, and using not only the mean of the signal, but also other statistics as an input feature for the classification algorithm.

2. Methods

Most fNIRS studies looking to classify certain groups or conditions consist on four main steps: (1) Collection of data from participants. (2) Pre-processing steps to convert raw intensity data into concentration changes and account for possible artifacts and physiological noise. (3) Extraction of the relevant information from the signal (feature extraction). (4) Classification of subjects depending on their features. Although all these steps were not performed for this report, the experimental conditions under which data was collected, the details about data pre-processing and the methodology used for extracting features and classification are described in this section.

2.1 Participants

The participants were matched on age and intelligence quotient (IQ). Subjects included 27 TD individuals (7 females and 20 males, mean age = 31.9 $\pm$ 12 years, full-scale IQ = 117 $\pm$ 13) and 26 subjects with high-functioning ASD (4 females and 22 males, mean age = 33.2 $\pm$ 10 years, full-scale IQ = 117 $\pm$ 13). Participants with ASD were diagnosed through expert clinical evaluation on Module 4 of the Autism Diagnostic Observation Schedule [20, 21].

2.2 Protocol

The experiment lasted one hour, during which participants were asked to perform a number of tasks under different scenarios. The study was divided into 12 blocks of 4 minutes each, between which subjects rested for 60 seconds. During the 8 PM blocks (Figure 3), subjects were asked to perform an action involving the prospective memory while doing another demanding task known as "ongoing task"(OG). On the other hand, during the other 4 blocks (OG blocks) participants kept performing the OG task without involving any PM task. For this study, the OG tasks consisted of either guessing whether the sum of two numbers resulted in an even or odd number, or if certain products cost more or less than £14. The PM task consisted of remembering to press the space-bar and to deposit a coin into a money box when participants felt that 30 seconds had passed. Each time a subject pressed the space-bar, a neural activation was expected in the PFC, and is therefore referred as a PM hit. In order to study the social aspects of the PM, in some of the PM blocks an experimenter was present in the room (audience effect, blocks 1,4,6 and 7), and the coins in the box could either be earned for the participants (blocks 3,4, 5 and 6) or for the experimenter (reward effect).

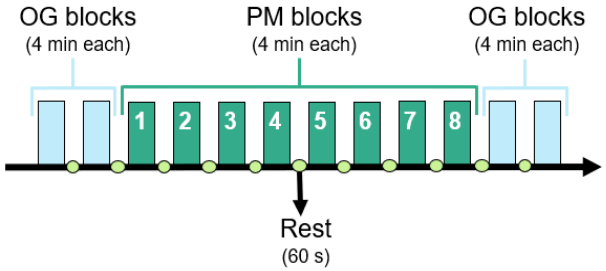

Figure 3. Experimental protocol diagram divided into 4 ongoing (OG) and 8 prospective memory (PM) blocks.

2.3 Functional NIRS recording and pre-processing

The WOT system (Hitachi High-technology Corporation, [22]) was used in order to record hemodynamic signals over the PCF. The headset of the fNIRS system covered the PFC, and contained 6 emitters and 6 detectors with a source-detector separation of 3 cm [23]. As shown in Figure 4, 16 channels were used as a measurement points at a sampling frequency of 5Hz. Each emitter generated two wavelengths, 705 and 830 nm, which enabled the measurement of both HbO_2 and HHb concentrations over time.

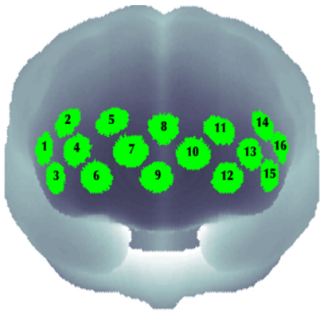

Figure 4. Arrangement of channels in the fNIRS probe.

Raw data was exported into MATLAB [24] for subsequent analyses. Pre-processing was carried out using Homer2 software package [25]. The fNIRS system used the MBLL (Equation 1) to convert changes in light intensity to optical density (OD). Then, in order to remove physiological noise and motion artifacts, the optical signal was first corrected with a wavelet-based approach [26] and band-pass filtered between 0.01 and 0.4 Hz. Finally, OD was converted to HbO_2 and HHb concentration data according to Equation 2.

2.4 Feature extraction

Characteristic properties of the fNIRS signal were calculated in order to summarize the information contained in a specified time-window. These properties are referred as features. For this project, HbO_2 and HHb concentration data were analysed in order to identify those features that better discriminated between ASD and TD subjects when performing a PM task. To do this, a number of experiments were performed to obtain the decoding accuracy when trying to classify subjects as TD or ASD depending on their activation patterns. For each experiment, a different feature was extracted for both signals, HbO_2 and HHb. Two main types of features were extracted:

Amplitude features: extracted from the signal around the PM hit (See Figure 5):

1. Mean.
2. Median.
3. Delta: Difference between the mean signal 5s after the PM hit and the mean 5s before the PM hit.
4. Standard deviation (Std).
5. Entropy: Shannon entropy of the signal.
6. Maximum: Peak of the hemodynamic signal during the PM hit.

Dynamic features: β-values obtained when applying the general linear model (GLM). For details about method see Worsley 1995 [27]:

1. Block-design: the 8 PM blocks were modelled as 4-mins blocks in the design matrix, and the contrasts (Experimenter Present vs Absent) and (Earning for Themselves vs Earning for Others) were computed. The β-values resulting from each of these two contrasts for each participant and channel were used as input features.
2. Event-related design: the PM hits within each PM block were modelled as 0-duration events in the design matrix, and the contrasts (Experimenter Present vs Absent) and (Earning for Themselves vs Earning for Others) were computed. The β-values resulting from each of these two contrasts for each participant and channel were used as input features.

Previous analyses performed by the research group indicated that activation patterns, on average, were best observable from 5s before to 5s after the PM hit. As a result, amplitude features were extracted in a time-window of 10s centred at the PM hit, for each subject, channel and hit (Figure 5). Noteworthy is that the number of PM hits per subject depended on how many times they pressed the space-bar, and was therefore not constant across subjects.

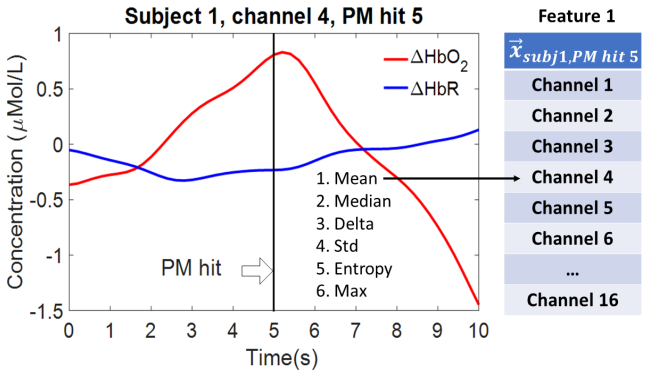

Figure 5. Example of multichannel pattern generation on amplitude features. The Figure shows HbO_2 and HHb signal in a time-window of 10s around the 5^{th} PM hit of subject 1 in channel 4.

Before applying the classification algorithm, a single vector of 16 cells was generated per each subject (where each cell contains the averaged feature for a particular channel) as proposed by Emberson 2017 [14]. In order to obtain this vector as an input for the classification algorithm, the same procedure was applied for each experiment involving amplitude features. First, as described in Figure 5 and Equation 3, the specified feature was extracted on each PM hit to generate a *multichannel pattern* per each subject, channel and PM hit:

$$\vec{x}_{Subject,PM_{hit}} = [x_1, x_2, x_3, ...x_{16}] \tag{3}$$

Then, *multichannel patterns* were averaged across all PM hits to obtain ***subject-level multichannel patterns***:

$$\vec{x}_{Subject} = \frac{1}{n_{hits}} \sum_{j=1}^{n_{hits}} \vec{x}_{Subject,PM_{hit}\,j} \tag{4}$$

Where n_{hits} is the total number of PM hits of each subject and $\vec{x}_{Subject}$ is a vector of 16 cells containing the averaged feature on each channel. For the experiments involving dynamic features, $\vec{x}_{Subject}$ was directly generated by extracting the β-values obtained when applying the GLM to each channel.

2.5 Classification

The classification method used in this study was adapted from Emberson 2017 [14]. As *subject-level multichannel patterns* could be generated for all features, the MVPA was applied in the same way for each one of the extracted features. It is important to note that the condition of each individual (TD or ASD) was known a priori, and the aim of this analysis was to investigate whether their condition could be correctly guessed by comparing their hemodynamic response with the other TD and ASD individuals.

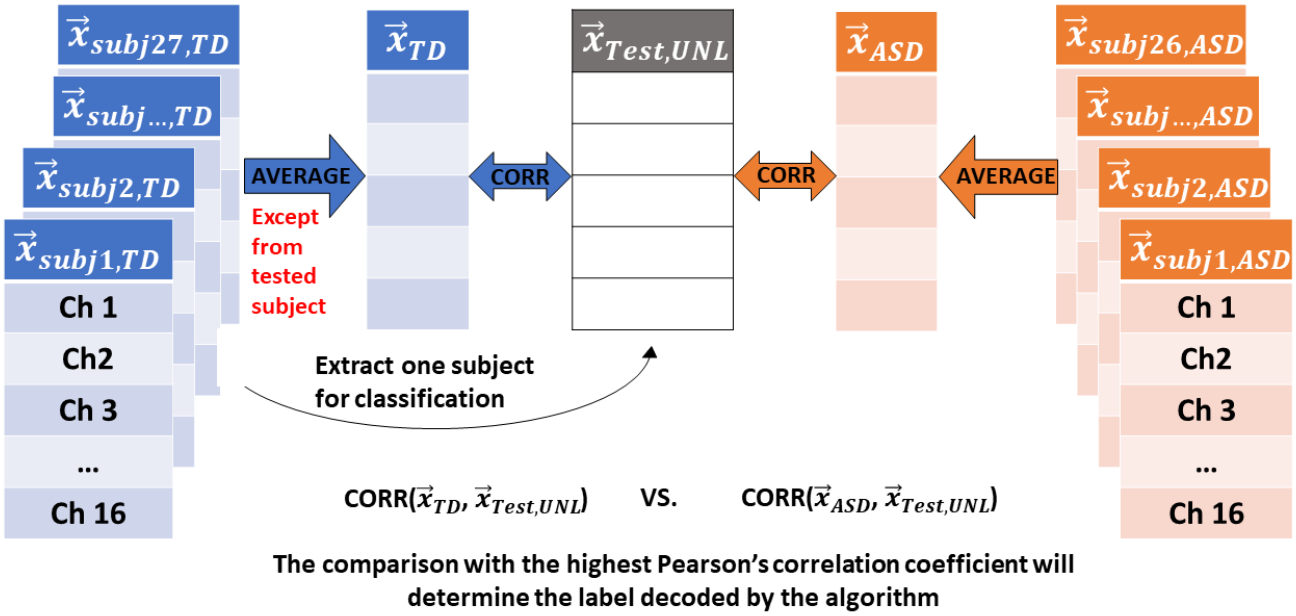

Figure 6. Illustration of the multivariate method applied to discriminate between TD and ASD participants depending on their hemodynamic patterns.

The MVPA involved decoding the condition of participants by comparing representational similarity structures by means of a simple Pearson's correlation coefficient. The steps involved in the classification approach are illustrated in Figure 6. First, subject-level multichannel patterns were labelled according to subject's condition, $\vec{x}_{Subject,Condition}$ (where *Condition* can be either TD or ASD). Subsequently, each subject was classified once at a time (leave-one-out method) by comparing their multichannel patterns with the average patterns of subjects with the same condition (group models). For instance, if the tested subject belonged to the TD group (example shown in Figure 6), two group models would be generated ($\vec{x}_{TD}$ and $\vec{x}_{ASD}$) by averaging the $\vec{x}_{Subject,Condition}$ across subjects with the same condition. However, when generating the $\vec{x}_{TD}$ group, the tested subject ($\vec{x}_{Test,UNL}$) would be removed from the average, and the group model for TD would be therefore formed by the average multichannel patterns of 27-1 subjects. Once the group models were generated, $\vec{x}_{Test,UNL}$ was compared to both, $\vec{x}_{TD}$ and $\vec{x}_{ASD}$ by computing the Pearson's correlation coefficient between $\vec{x}_{Test,UNL} - \vec{x}_{TD}$ and $\vec{x}_{Test,UNL} - \vec{x}_{ASD}$. Then, the comparison with the highest correlation coefficient would determine the label of the tested subject. If the label decoded by the classification algorithm corresponded to the original label of the tested subject, then decoding of this individual was considered successful. This process was iterated 53 times, so that each individual acted as a test subject and was classified using the approach described.

Since in each iteration a different subject was left out from the average group in each iteration, 53 different group models were recomputed using the non-tested individuals. Once all subjects were tested, the number of successfully decoded participants was divided by 53 to obtain the total classification accuracy.

Subsets of channels It is important to note that the input vectors of the classification method previously described, $\vec{x}_{Subject,Condition}$, all had the same length, 16 cells, in which each cell was generated from the information of a single channel. Therefore, it was also possible to study how effective classification resulted when only a certain subset of channels was considered. It can be hard to determine how many channels (and which ones) should be included in a subset when aiming to maximize decoding accuracy. However, due to the relatively small number of channels, all possible permutations were studied. The subset sizes were increased from 2 to 16, and all possible permutations of channels were studied for each subset size. The number of possible permutations (C) of channels (n,16) by a given subset size (k) is determined by the binomial coefficient (Equation 5). As k was varied from 2 to 16, the total number of channel permutations was equal to 65,519.

$$C(n,k) = \frac{n!}{k!(n-k)!} \tag{5}$$

The simplicity of the MVPA used in this study made the exhaustive combinatorial analysis computationally fast. Moreover, the fact that all accuracies were computed for each permutation enabled to study whether particular subset sizes were more optimal for classification.

3. Results

As previously mentioned, in each experiment a different feature was extracted, and decoding accuracy was assessed for each permutation of channels. The results of this classification were separately calculated for HbO_2 and HHb, and extracted into a box-plot (Figure 7). In each box, the edges determined the 25th and 75th percentiles, whereas the central red mark was the median accuracy for that subset size. Whiskers extended until the extreme data points not considered outliers, and the outliers were individually plotted in red using the '+' symbol. Figure 7 shows the classification accuracy from the MVPA applied using the feature Delta in the HbO_2 signal. In this plot, accuracies were displayed per subset size, which increased from 2 to 16 channels. It is worth noting that for a subset size of 16 channels there was just one possible group, whereas for subset sizes around 8 channels the number of possible permutations was much larger.

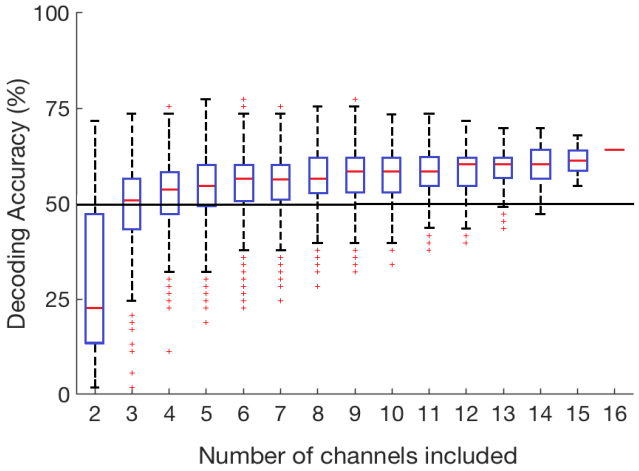

Figure 7. Decoding accuracy for the different subsets of channels used in the classification approach. This box-plot displays the results obtained extracting the feature Delta from the HbO_2 signal.

Box plots as the one in Figure 7 were obtained for each experiment and signal. The information from each one of the obtained graphs was summarized in Table 1. Two main results were included for each signal. First, the best median accuracy from the box-plot was included together with the number of channels (subset size) required to obtain it. Then, the best accuracy obtained over all the permutations was included with its discriminant subset. As it can be observed, the best median accuracy (64.2%) was obtained when extracting Delta from the HbO_2 signal. Therefore, in order to visualize spatially distributed patterns of activation, the channels that best performed on the classification task for Delta were highlighted in Figure 8a for the HbO_2 and Figure 8b for the HHb.

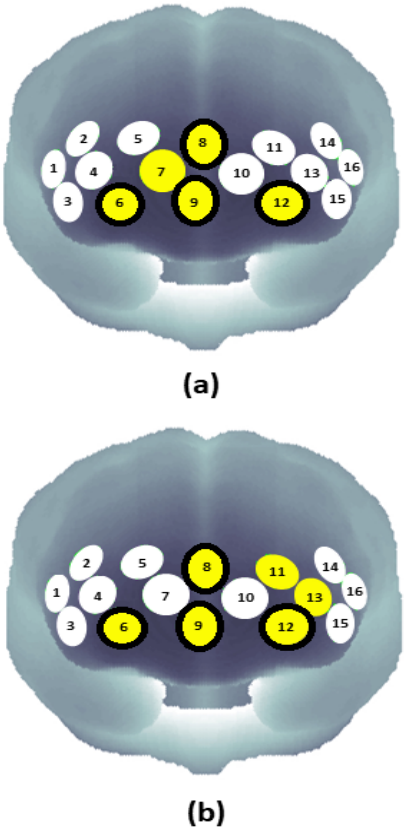

Figure 8. Subsets of channels that best performed in the classification task between TD and ASD groups when using Delta as an input feature. Highlighted channels show the best subsets for the (a) HbO_2 and (b) HHb signal. Channels that were present in both cases are encircled in black.

4. Discussion

First of all, general results obtained in this study were compared to the ones exposed by Emberson [14] since the same classification approach (RSA) was used. There, 10 channels were used to decode visual and auditory stimulus in infants, and it was observed that median decoding accuracy always improved when increasing the subset size. However, as only 10 channels were used in the study, it is interesting to analyse whether decoding accuracy is likely to keep increasing when incorporating more than 10 channels or if there is an optimal subset size for the RSA approach. Here, this was studied by performing all combinations of channels. Figure 7 shows how median accuracy kept increasing when incorporating from 2 to 16 channels. In Table 1 it can be observed that for those experiments obtaining best median accuracies above 55%, this was mostly achieved with either 15 or 16 channels, and a similar pattern from the one in Figure 7 was displayed in their box-plots. These results suggest that on average, when using 16 or less channels for fNIRS decod-

Table 1. Decoding accuracies for each feature (expressed in % of successfully classified subjects). Results from the classification approach were reported for both signals, HbO_2 and HHb. After applying the MVPA to all possible combinations of channels, the best median accuracy and the maximum accuracy were summarized in this table.

	HbO_2		HHb	
Features	Best median accuracy (subset size)	Best accuracy (subset)	Best median accuracy (subset size)	Best accuracy (subset)
Mean	57.6 (15)	77.4 (1 4 9 10 16)	51 (4)	71.7 (2 3 4 6 7 9 12 14)
Median	58.5 (16)	75.5 (3 9 12 14 15 16)	51 (5)	67.9 (1 6 8)
Delta	64.2 (16)	77.4 (6 7 8 9 12)	56.6 (8)	77.4 (6 8 9 11 12 13)
Standard deviation	51 (16)	69.8 (1 4 12 13 16)	58.5 (16)	71.7 (2 5 6 10 13 15)
Entropy	54.8 (13)	70 (1 3 4 11 13 14 16)	58.5 (15)	71.7 (2 4 15)
Maximum	45.3 (16)	66 (5 10 13 15)	60.4 (16)	71.7 (1 2 4 7 15 16)
Event Design-Reward	60.4 (16)	79.2 (2 8 9 15)	45 (3)	64.2 (2 6 8 10 15)
Event Design-Audience	51 (16)	67.9 (2 8 10 15)	49 (5)	73 (4 5 9 11 12)
Block Design-Reward	53 (14)	74 (1 5 12 13 15)	45 (16)	70 (4 7 8 10 11 12)
Block Design-Audience	45 (3)	68 (1 2 4 9 13 15)	54 (5)	71.7 (8 10 12 14 15)

ing, representational similarity analyses would benefit from increasing the number of channels included in the structure. It is worth noting that Emberson reported much higher decoding accuracies, as classifying atypical populations represents a more challenging task due to the high degree of variability across subjects. Moreover, the sample size used in this study contained 53 participants instead of 19, which can be more affected by other sources of variation.

In general, median accuracies ranged from 45 to 64.2% and the best subsets in each experiment reported accuracies between 64.2 and 79.2% (Table 1). The best subsets differed across experiments, and thus made the maximum accuracies less reliable. However, the fact that some specific features reported median accuracies above 60% suggests that subtle differences in activation patterns were present and detected by the MVPA. From the results obtained when using amplitude features, a certain pattern was detected. Interestingly, whereas the mean, median and Delta seemed to better discriminate subjects when using the HbO_2 response, the standard deviation, entropy and maximum of the signal seemed to better decode subjects with the HHb signal. Although this evidence is not conclusive, these results suggest that when extracting features from the data, measures of central tendency might be more informative for the HbO_2 signal while statistics measuring dispersion might detect more significant differences between groups when using HHb.

Out of all the experiments tested, Delta was considered to be the most informative feature. Apart from reporting the highest median accuracy, subsets that better decoded subjects in HBO_2 and HHb shared many channels (see Figure 8). This is an important result to take into account when evaluating discriminant channels. Due to their physiological relation, one might expect to see correlation between oxy and deoxy hemoglobin (when one increases the other decreases). Therefore, the fact that 4 channels (6, 8, 9 and 12) were present in the best subset for both signals adds robustness to the results reported by this feature. As Delta measures the difference between the average signal before and after the PM hit, these results suggest that individuals with ASD might present differences in neural activation before and after prospective memory tasks compared to TD subjects. In addition, it is important to note that the most discriminant channels in this study were not located in bilateral regions of the PFC but on the central area. Although previous studies reported atypical activation of the right PFC in ASD subjects [11, 12] this was not detected in this study. Therefore, more analyses should be performed to contrast these results.

From the experiments using dynamic features, the Even-Design under the reward effect with the HBO_2 signal, resulted to be the one with the best performance, including the best overall accuracy (79.2%) successfully decoding 42 of the 53 participants. Also, in this case, channels 8 and 9 were included in the best subset (both present in Figure 8). Due to the fact that the other dynamic features reported relatively low accuracies it was not possible to speculate whether analysing the signal over whole block was better than focusing on the PM hits (events). However, it was shown that traditional methods based on the GLM can be combined with MVPA approaches to provide features of the signal.

Conclusions and future work This study aimed to identify characteristic activation patterns of subjects with ASD when performing prospective memory tasks by analysing their fNIRS signal. A simple correlation-based MVPA was applied to classify TD and ASD depending on their hemodynamic response. The approach was computationally fast, it exhibited the potential of MVPA on atypical populations using fNIRS

and allowed the study of spatially distributed patterns. Similarly to Emberson et al. 2017, the results obtained showed that in general, RSA benefits from increasing the number of channels included in the structures. Moreover, analysing both HBO_2 and HHb enabled to contrast results and to identify certain statistics that better classified subjects when using one signal or another. Several features were extracted, and differences of the signal before and after the prospective memory task proved to be the most robust and discriminant approach. Finally, larger differences between ASD and TD were observed in the central regions of the prefrontal cortex rather than in the bilateral areas. This result is not consistent with previous studies and it reflects the need for further analyses.

Even though the method has proven to be easy to interpret, informative and effective to study spatial distributions, the development of diagnostic tools for ASD will require to improve the accuracy in the classification approach and more robust results will be needed to extract general conclusions. Several studies have started to apply machine-learning approaches to fNIRS. Although machine learning classifiers are particularly suited to detect hidden patterns in the data, they also present computational costs and more barriers on their interpretation. However, the MVPA used in this study might provide a fast-initial analysis into the feature space that can be included into machine learning algorithms. Future studies will analyse this data using machine-learning approaches and study whether neuroimaging data can be integrated with behavioural results to provide a robust biomarker.

Acknowledgments

Dr. Paola Pinti, for her extensive support throughout the project and all the fruitful meetings and discussions. Dr. Ilias Tachtsidis for providing instruction in the writing-up and a critical perspective of the results obtained.

References

[1] American Psychiatric Association. *Diagnostic and Statistical Manual of Mental Disorders*. 2013.

[2] Yusuke Moriguchi and Kazuo Hiraki. Prefrontal cortex and executive function in young children: a review of NIRS studies. *Frontiers in Human Neuroscience*, 7, 2013.

[3] Christine Ecker, Vanessa Rocha-Rego, Patrick Johnston, Janaina Mourao-Miranda, Andre Marquand, Eileen M. Daly, Michael J. Brammer, Clodagh Murphy, and Declan G. Murphy. Investigating the predictive value of whole-brain structural MR scans in autism: A pattern classification approach. *NeuroImage*, 49(1):44–56, 2010.

[4] Christine Ecker and Declan Murphy. Neuroimaging in autism - from basic science to translational research. *Nature Reviews Neurology*, 10:82–91, 2014.

[5] Evdokia Anagnostou and Margot J. Taylor. Review of neuroimaging in autism spectrum disorders: What have we learned and where we go from here, 2011.

[6] Sam J. Gilbert, Julia D.I. Meuwese, Karren J. Towgood, Christopher D. Frith, and Paul W. Burgess. Abnormal functional specialization within medial prefrontal cortex in high-functioning autism: A multi-voxel similarity analysis. *Brain*, 132(4):869–878, 2009.

[7] Paola Pinti. *Lighting up the brain: Exploring fNIRS portability and systemic effects*. PhD thesis, Università degli Studi "G. d'Annunzio", 2015.

[8] Ilias Tachtsidis and Felix Scholkmann. False positives and false negatives in functional near-infrared spectroscopy: issues, challenges, and the way forward. *Neurophotonics*, 3(3):031405, 2016.

[9] Felix Scholkmann, Felix Scholkmann, Stefan Kleiser, Andreas Jaakko, Raphael Zimmermann, Juan Mata, Ursula Wolf, and Martin Wolf. A review on continuous wave functional near- infrared spectroscopy and imaging instrumentation and methodology instrumentation and methodology. *NeuroImage*, 85(May):6–27, 2014.

[10] Noman Naseer and Keum-Shik Hong. fNIRS-based brain-computer interfaces: a review. *Frontiers in Human Neuroscience*, 9(January), 2015.

[11] Akira Yasumura. Neurobehavioral and Hemodynamic Evaluation of Cognitive Shifting in Children with Autism Spectrum Disorder. *Journal of Behavioral and Brain Science*, 02(04):463–470, 2012.

[12] Ting Xiao, Zhou Xiao, Xiaoyan Ke, Shanshan Hong, Hongyu Yang, Yanli Su, Kangkang Chu, Xiang Xiao, Jiying Shen, and Yijun Liu. Response Inhibition Impairment in High Functioning Autism and Attention Deficit Hyperactivity Disorder: Evidence from Near-Infrared Spectroscopy Data. *PLoS ONE*, 7(10), 2012.

[13] Kenneth A. Norman, Sean M. Polyn, Greg J. Detre, and James V. Haxby. Beyond mind-reading: multi-voxel pattern analysis of fMRI data, 2006.

[14] Lauren L. Emberson, Benjamin D. Zinszer, Rajeev D.S. Raizada, and Richard N. Aslin. Decoding the infant mind: Multivariate pattern analysis (MVPA) usingfNIRS. *PLoS ONE*, 12(4), 2017.

[15] Dominic Heger, Reinhard Mutter, Christian Herff, Felix Putze, and Tanja Schultz. Continuous recognition of affective states by functional near infrared spectroscopy

signals. *Proceedings - 2013 Humaine Association Conference on Affective Computing and Intelligent Interaction, ACII 2013*, pages 832–837, 2013.

[16] S. M.Hadi Hosseini, Yoko Mano, Maryam Rostami, Makoto Takahashi, Motoaki Sugiura, and Ryuta Kawashima. Decoding what one likes or dislikes from single-trial fNIRS measurements. *NeuroReport*, 22(6):269–273, 2011.

[17] Tadanobu Misawa, Tetsuya Shimokawa, and Shigeki Hirobayashi. Possibility for Predicting the Evaluation of Product Price in the Prefrontal Cortex : A NIRS Study. *International Journal of Engineering and Innovative Technology*, 4(3):153–160, 2014.

[18] Hiroko Ichikawa, Jun Kitazono, Kenji Nagata, Akira Manda, Keiichi Shimamura, Ryoichi Sakuta, Masato Okada, Masami K. Yamaguchi, So Kanazawa, and Ryusuke Kakigi. Novel method to classify hemodynamic response obtained using multi-channel fNIRS measurements into two groups: exploring the combinations of channels. *Frontiers in Human Neuroscience*, 8(July):1–10, 2014.

[19] T. J. Huppert, R. D. Hoge, S. G. Diamond, M. A. Franceschini, and D. A. Boas. A temporal comparison of BOLD, ASL, and NIRS hemodynamic responses to motor stimuli in adult humans. *NeuroImage*, 29(2):368–382, 2006.

[20] C Lord, S Risi, L Lambrecht, E H Jr Cook, B L Leventhal, P C DiLavore, a Pickles, and M Rutter. The Autism Diagnostic Schedule – Generic: A standard measures of social and communication deficits associated with the spectrum of autism. *Journal of Autism and Developmental Disorders*, 30(3):205–223, 2000.

[21] K. Gotham, A. Pickles, and C. Lord. Trajectories of Autism Severity in Children Using Standardized ADOS Scores. *Pediatrics*, 130(5):e1278–e1284, 2012.

[22] Hirokazu Atsumori. Noninvasive imaging of prefrontal activation during attention-demanding tasks performed while walking using a wearable optical topography system. *Journal of Biomedical Optics*, 15(4):046002, 2010.

[23] Paola Pinti, Clarisse Aichelburg, Frida Lind, Sarah Power, Elizabeth Swingler, Arcangelo Merla, Antonia Hamilton, Sam Gilbert, Paul Burgess, and Ilias Tachtsidis. Using Fiberless, Wearable fNIRS to Monitor Brain Activity in Real-world Cognitive Tasks. *Journal of Visualized Experiments*, (106):1–13, 2015.

[24] The MathWorks. MATLAB (R2017b), 2017.

[25] Sven Heinz, Christopher Benner, Nathanael Spann, Eric Bertolino, Yin C. Lin, Peter Laslo, Jason X. Cheng, Cornelis Murre, Harinder Singh, and Christopher K. Glass. Simple Combinations of Lineage-Determining Transcription Factors Prime cis-Regulatory Elements Required for Macrophage and B Cell Identities. *Molecular Cell*, 38(4):576–589, 2010.

[26] Behnam Molavi and Guy A. Dumont. Wavelet-based motion artifact removal for functional near-infrared spectroscopy. *Physiological Measurement*, 33(2):259–270, 2012.

[27] K. J. Worsley and K. J. Friston. Analysis of fMRI time-series revisited — Again. *NeuroImage*, 2(3):173–181, 1995.